CARBON 50 (2012) 659–667

Available at www.sciencedirect.com

SciVerse ScienceDirect

journal homepage: www.elsevier.com/locate/carbon

Annealing a graphene oxide film to produce a free standing high conductive graphene film

Cheng-Meng Chen [a,d], *Jia-Qi Huang* [b], *Qiang Zhang* [b,*], *Wen-Zhao Gong* [a], *Quan-Hong Yang* [c], *Mao-Zhang Wang* [a], *Yong-Gang Yang* [a,*]

[a] *Key Laboratory of Carbon Materials, Institute of Coal Chemistry, Chinese Academy of Sciences, Taiyuan 030001, China*

[b] *Beijing Key Laboratory of Green Chemical Reaction Engineering and Technology, Department of Chemical Engineering, Tsinghua University, Beijing 100084, China*

[c] *Key Laboratory for Green Chemical Technology of Ministry of Education, School of Chemical Engineering and Technology, Tianjin University, Tianjin 300072, China*

[d] *Graduate University of Chinese Academy of Sciences, Beijing 100049, China*

ARTICLE INFO

Article history:
Received 6 July 2011
Accepted 12 September 2011
Available online 17 September 2011

ABSTRACT

A free-standing graphene oxide film (GOF) obtained by self-assembly at a liquid/air interface was annealed in a confined space between two stacked substrates to form a free-standing highly conductive graphene film. Characterization indicates that the oxygen-containing functional groups (e.g. epoxy, carboxyl, and carbonyl) were removed as small molecules (e.g. H_2O, CO_2, and CO) during the annealing, meanwhile the size of sp^2 domains in the film was decreased. When annealed between two stacked wafers, random interlayer expansion and fractional movement in the GOF were suppressed by the pressure-induced friction, which helps preserve the morphology of the film. The conjugation in the basal plane of graphene and π–π interactions between well stacked graphene sheets favor the transportation of charge carriers in the film, to produce a good electrical conductivity of the resulting free-standing reduced GOF (increased from 1.26×10^{-5} to 272.3 S/cm).

1. Introduction

As a two-dimensional crystal of sp^2 conjugated carbon atoms, graphene is considered to be the mother of all graphitic allotropes including zero-dimensional fullerenes, one-dimensional carbon nanotubes, and three-dimensional (3D) graphite [1]. It possesses a large surface area (2630 m^2/g in theory), high electric charge carrier mobility ($\mu = 1.5 \times 10^4\ cm^2 V^{-1} s^{-1}$), and excellent mechanical strength (tensile strength 130 GPa). However, similar to most nanocarbon materials, graphene also suffers from the bottleneck of complex and inconvenient handling process for industrial applications. Thus, in order to fully demonstrate the prominent properties of graphene, the integration of individual graphene sheets into macroscopic 3D assemblies is highly concerned [2–4]. Various 3D graphene architectures have been constructed, such as graphene oxide (GO) [5–7] and/or graphene films [8–11], hydrogel [12], sponges [10], and foams [13–16]. With unique mechanical, electronic, and optical property, these materials hold great potential for applications in composites, batteries, supercapacitors, electronics, and sensors [7–9,11,13–18]. As developed by Ruoff and co-workers, GO films (GOFs), with a unique layered structure and a tensile strength of 45–135 MPa, can be easily fabricated by flow directional assembly of GO sheets. The material exhibits attracting prospect for applications in films with controlled permeability, anisotropic ionic conductors and supercapacitors [5]. Besides, macroscopic 3D graphene foams fabricated by a template-directed chemical vapor deposition

---

[*] *Corresponding authors:* Fax: +86 10 6277 2051.
E-mail addresses: zhang-qiang@mails.tsinghua.edu.cn (Q. Zhang), yangyg@sxicc.ac.cn (Y.-G. Yang).

0008-6223/$ - see front matter © 2011 Elsevier Ltd. All rights reserved.
doi:10.1016/j.carbon.2011.09.022

also possess a unique network structure with outstanding electrical and mechanical properties [15]. Thus, developing an effective and efficient method for free-standing graphene film is an important issue for the further exploration towards the property as well as the large-volume applications of graphene.

Among various physical and chemical synthesis approaches, oxidative intercalation and exfoliation of natural graphite, followed by thermal or chemical reduction has been evaluated to be a strategic starting point for low-cost, large-scale production of graphene materials [2–4]. Meanwhile, the as-obtained chemically derived graphene sheets can be conveniently deposited on any substrate. Up to now, large area GOFs can be easily obtained by simple solution process such as filtration [5,8,9,11,19], spray coating [20], spin casting [21], Langmuir–Blodgett assembly [22], and self-assembly at the liquid/air interface [6]. However, the as-obtained GOFs are almost insulating. Thus, in order to restore the conductivity of GOFs, various deoxygenating approaches on GO powder or film have been explored, which can be roughly sorted as the “dry” processes (high temperature annealing in vacuum, inert, or reductive atmosphere [20,23–25]) and the “wet” processes (chemical reduction by strong agents in solution, such as hydrazine [20,26,27], sodium borohydride [28], hydrohalic acid [29], aluminum powder [30], the sequential use of sodium borohydride and sulfuric acid [31]). However, the GOFs, especially for the free-standing ones, are easily to be delaminated and thus cannot maintain the film-like morphology during the intensive reduction process. Therefore, a simple way for the reduction of GOF should be explored to maintain its free-standing film-like morphology as well as to achieve high electric conductivity. In this contribution, a free-standing GOF obtained by self-assembly at a liquid/air interface was annealed in a confined space between two stacked substrates to form a free-standing highly conductive graphene film.

2. Experimental

GO was prepared by a modified Hummers method which is similar to our previous report [6,32]. GO powder (3.0 g) was suspended in 1.0 L of diluted water, followed by a 30-min ultrasonication in a cleaner bath (200 W). The above brownish solution was further centrifuged at 4000 rpm for 10 min to get rid of the small amount of impurities and inadequate exfoliated GO stacks. Thus, a stable hydrosol of GO with a concentration of ~2.8 mg/mL was obtained. To prepare the GOF, the above hydrosol was heated at 80 °C for 40 min, during which a smooth and condensed thin film with a thickness of *ca.*

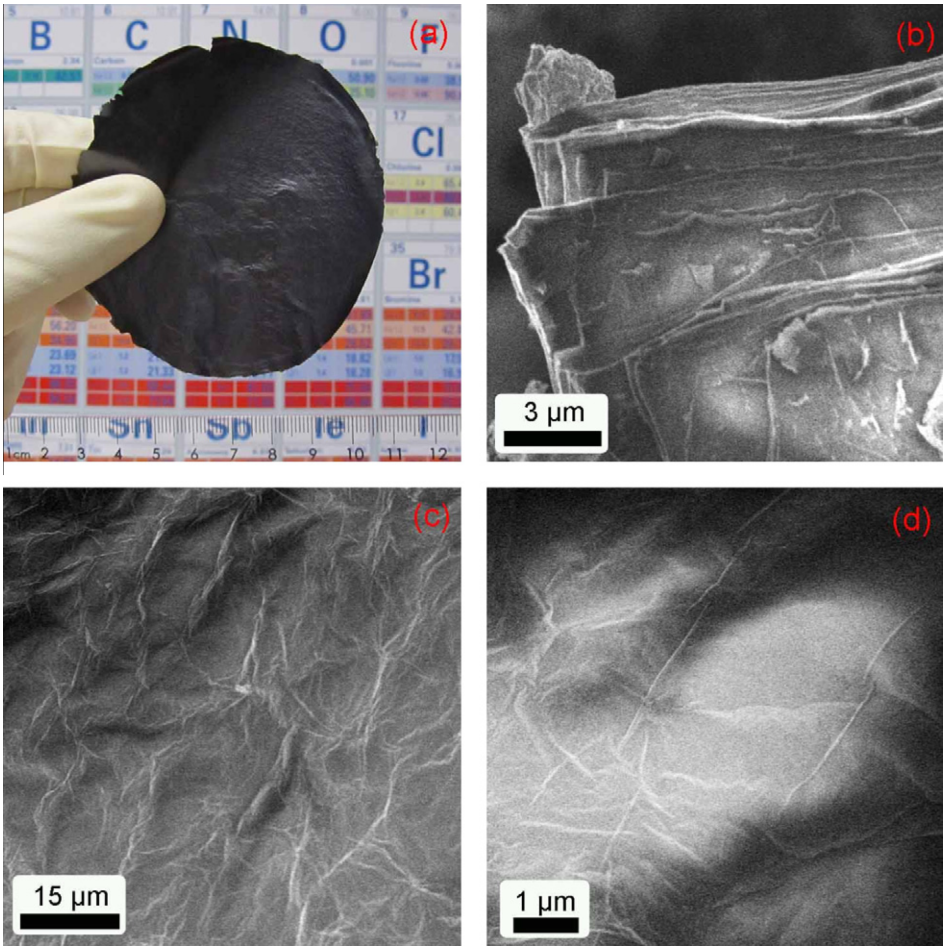

Fig. 1 – (a) Photographs and (b–d) SEM images of flexible GOFs produced through a self-assembly process at the liquid/air interface.

Table 1 – Summary of the structure and property of GOF and RGF.

Sample	C (wt.%)[a]	O (wt.%)[a]	C/O atom ratio[a]	I_D/I_G[b]	Residue Carbon (wt.%)[c]	Conductivity (S/cm)[d]
GOF	51.6	46.2	1.49	1.02	44.2	1.26×10^{-5}
RGF	92.4	7.1	17.3	1.38	84.5	272.3

[a] Obtained from XPS.
[b] Obtained from the Raman spectra.
[c] Obtained from TGA in argon atmospheres.
[d] Obtained by a four-probe method.

10 μm was formed gradually at the liquid/air interface. The as-obtained GOF was collected from the liquid–air interface and air dried at 80 °C for another 8.0 h to form a free-standing film. In order to restore the conductivity of the GOF, the film was laid between two stacked Si wafers. In contrast, another control sample was placed freely without the confinement of

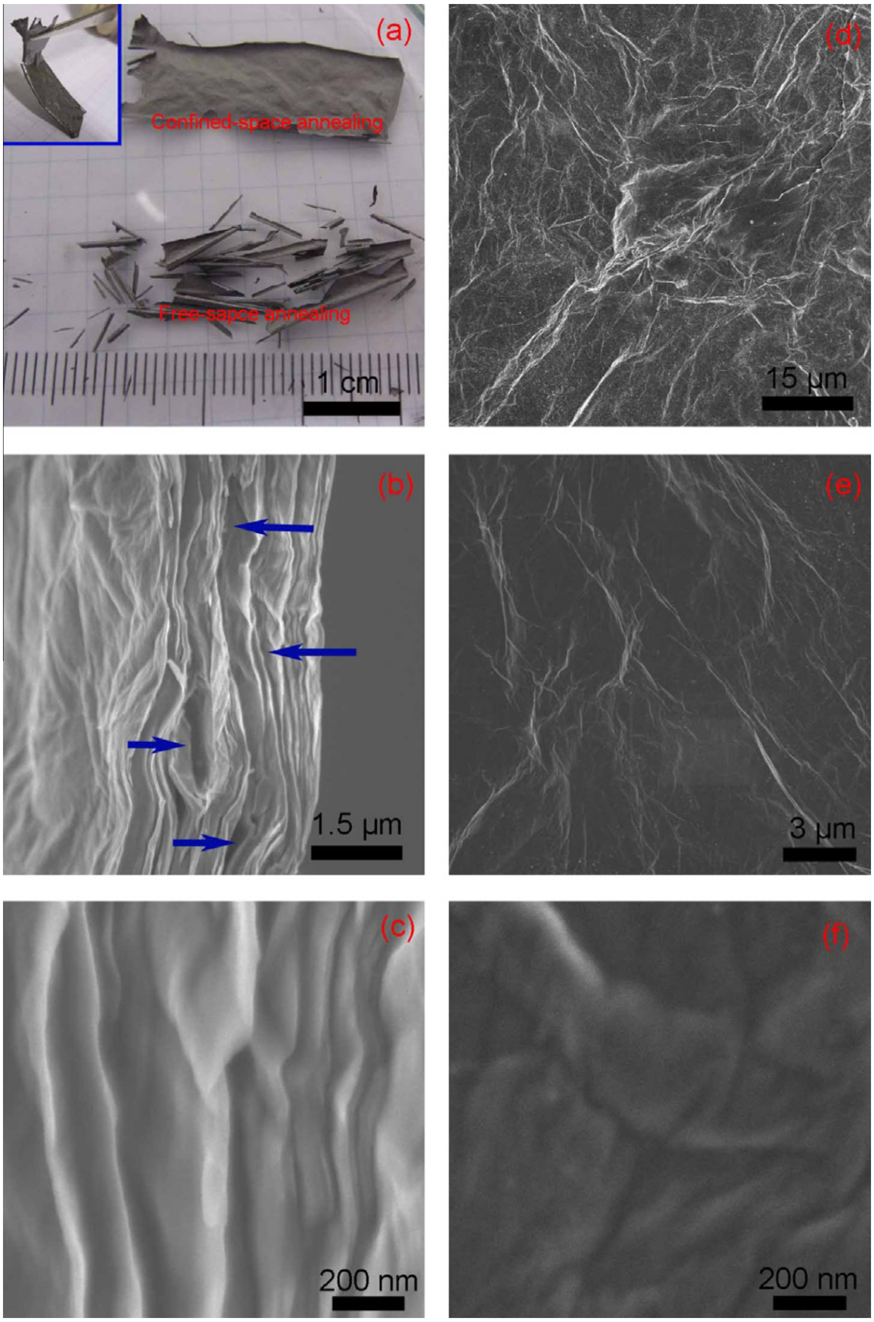

Fig. 2 – (a) Photographs of RGF annealed between two stacked substrates and RGX on the top surface of a wafer; the RGF is flexible, illustrated by the inserted photo; (b–f) SEM images of free-standing RGF annealed between two stacked substrates.

an upper wafer. Both the two samples were set into a horizontal tubular furnace, and the temperature was ramped from room temperature to 800 °C at a heating rate of 5 °C/min under the gas flow of argon (80 mL/min), and then dwelled at 800 °C for another 2.0 h for further deoxidation. During the annealing process, the film confined by two wafers maintained a very well free-standing morphology of flexible film, while the other one which was annealed freely without confinement finally collapsed into small fragments. Afterwards, the tube was cooled down to room temperature in argon atmosphere. The reduced graphene films with integrated morphology obtained from the confined space are denoted as RGF, while the cracked fragments from films annealed freely without confinement were denoted as RGX.

The as-obtained GOF, RGF, and RGX were characterized using scanning electron microscopy (SEM, JSM 7401F, 3.0 kV), Raman spectrophotometer (Renishaw RM2000 with laser excitation line at 633.0 nm), X-ray diffraction (XRD, Cu K_α radiation, D8 Advance, BRUKER/AXS, Germany), Fourier transform infrared spectroscopy (FT-IR) spectroscopy (IR200, Thermo Nicolet, US), X-ray photoelectron spectroscopy (XPS, PHI Quantera SXM), and thermal gravimetric analysis (TGA) system (STA 409PC luxx, Netzsch, Germany) equipped with a sweep gas mass spectroscopy appliance (ALZERS OmniStar 20, Switzerland). The electric conductivity of the film was performed on a Tongchuang SZT-2 Test Unit using a four-point-probe head with a pin-distance of about 1 mm.

3. Results and discussion

When the GO hydrosol was heated to 80 °C for 40 min, a smooth and condensed thin film with a diameter of 8.5 cm and a thickness of 10 μm was formed very rapidly at the liquid/air interface. The film can be easily separated from the parent GO suspension by decanting the residual suspension into another beaker, and a free-standing GOF was available after drying (Fig. 1a). As shown in the cross-sectional SEM image (Fig. 1b), the GOF exhibits a compact layer-by-layer stacking structure. The top surface SEM images shown in Fig. 1c and d indicate GO flakes served as 'building blocks' for the film. During the heating process, Brownian motion of GO sheets in the hydrosol is boosted. Thus, the GO sheets were prone to collide and interact with each other and move up to the liquid/air interface, where the water is spilling out from the hydrosol. The GO sheets tended to aggregate and assemble along the liquid/air interface. The nascent GO film will then capture the other GO sheets through interlayer van der Waals forces and began to stack. As a result, layer-by-layer film with ordered stacking morphology was formed [6]. As shown in Fig. 1, the GOF is of relatively smooth surface. Attributed to the poor conductivity of GOF (as shown in Table 1, $\sigma_S = 1.26 \times 10^{-5}$ S/cm), the charging behavior was observed during the SEM characterization.

After the annealing of GOF in argon atmosphere between two stacked Si wafers, a flexible free-standing graphene film were obtained (Fig. 2a). The RGFs are with shining metallic luster due to the increase in reflectivity of visible light. The electrical conductivity of RGF, as determined by a 4-probe method, was increased to 272.3 S/cm, which is 7 magnitude higher than that of raw GOF (Table 1). However, the film became fatigue and easily crushed into small debris. If the GOF was annealed in a free space without confinement by the upper substrate, the as-obtained film would crack itself into several small pieces (1–3 mm width and 5–15 mm in length, as shown in Fig. 2a) due to the random volume expansion in the annealing process. As indicated by the cross-sectional SEM images (Fig. 2b and c), the RGF maintains a well morphology of layer-by-layer packing of chemical derived graphenes. Narrow pores (indicated by the blue arrow in the Fig. 2b) were found in the RGF. The top surface of graphene sheets became coarse (Fig. 2d–f), and the graphene sheets were crampled with many wrinkles. As RGF possesses good electronic conductivity, no electron charging phenomena was observed.

XRD, Raman Spectroscopy, FT-IR, XPS, and TG-DSC-MS were employed to investigate the structural evolution during the annealing process. The diffraction peak was shifted from 12.6° of GOF to 26.1° of RGF, which exhibits a significant shrinking in lattice space (d_{002}) from 0.702 to 0.341 nm (Fig. 3a). This is attributed to the gradual removal of interlayer species such as physically adsorbed water and oxygen func-

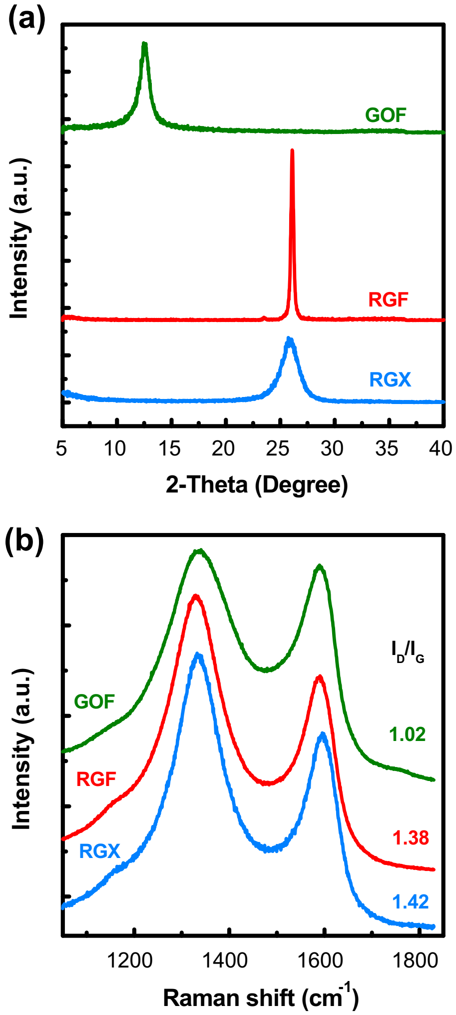

Fig. 3 – (a) XRD patterns and (b) Raman spectra of GOF, RGF, and RGX.

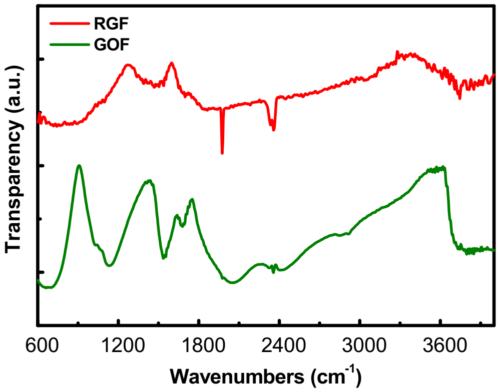

Fig. 4 – FT-IR spectra of GOF and RGF.

tionalities during annealing. The RGX exhibits a single peak around 26°, however, the diffraction intensity of which is quite lower comparing with the confined annealed ones, which implies a lower graphitization due to random interlayer expansion during annealing. When the filtrated GOF was annealed at 150 °C, the interlayer space between reduced GO flakes (d_{002} value) was 0.441 nm [33]. The d_{002} value decreased as the annealing temperature increased. The packing of graphene sheets in RGF annealed at 800 °C were more compact than that of HI reduction (0.357 nm) [29], $NaBH_4$ reduction (0.373 nm) [28], HI-AcOH reduction (0.362 nm) [34], but relatively larger than that of graphite (0.337 nm) [35]. This indicated that most of the functional groups had been removed at high annealing temperature. This was further confirmed by the fact that the 800 °C annealed RGF were with a high C/O ratio of 17.3. The D-band around 1335 cm^{-1} (corresponding the defects or edges) and G-band around 1588 cm^{-1} (corresponding to the first-order scattering of the E_{2g} mode [25]) were presented in Fig. 3b. After annealing, the D-band down shifted to 1328 cm^{-1}, while the intensity ratio of D- to G-band was increased from 1.02 to 1.38. The I_D/I_G ratio of as-obtained film debris (RGX) by annealing GOF in a free space (1.42) is a little higher than that of RGF (1.38). During annealing of GO film, the loss of carbon atoms from the graphene oxide lattice results in the formation of defects such as vacancies and distortions, and this separated an integrate sp^2 domain into several smaller sp^2 crystallines. Thus, the increase of the intensity ratio of D- to G-band was attributed from the numerous small sp^2 domains in the RGF. This phenomenon is similar to the reduction of GO by hydrazine hydrate [26,36], $NaBH_4$ [28], or HI solution [29] as reported in literatures.

The loss of oxygen-containing groups after annealing was confirmed by FT-IR spectrum. As shown in Fig. 4, the intensity of peak at 1150 cm^{-1} (–CO– groups), 1533 cm^{-1} (–COO– group), 1682 cm^{-1} (–COOH group), and 3700 cm^{-1} (–OH group) (identification similar to that reported in Refs. [37,38]) were significantly decreased. The evolution of functionalization in the film surface was further determined by XPS. As shown in Table 1, the relative contents of C and O elements were quanti-

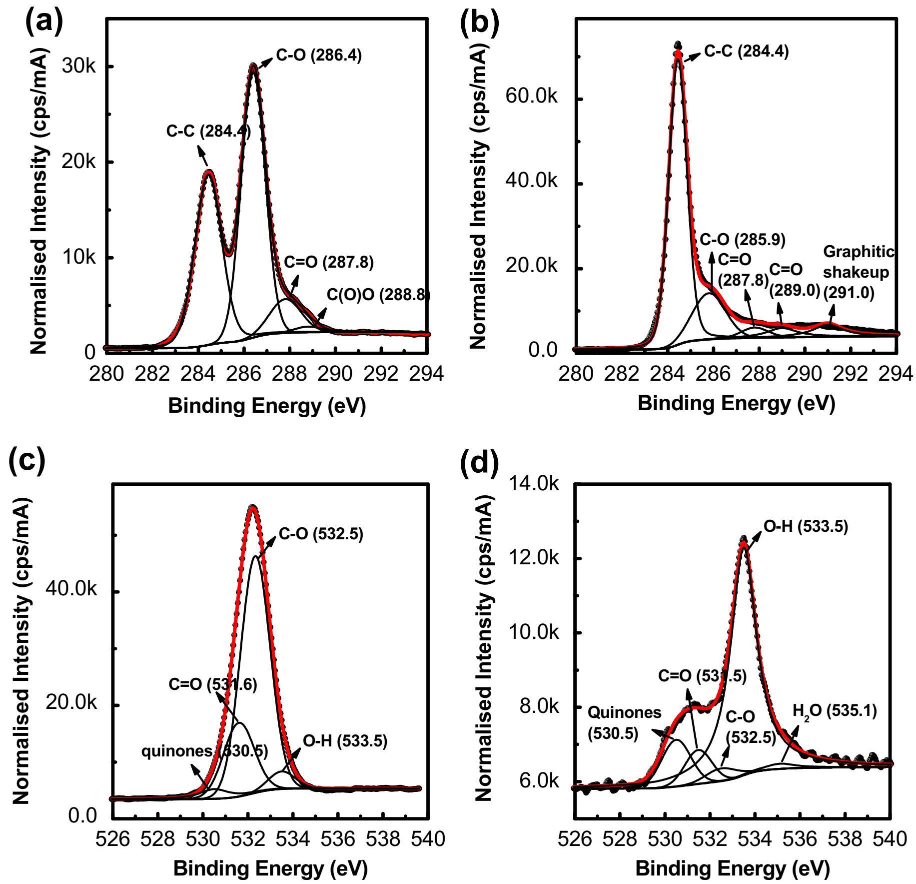

Fig. 5 – XPS elemental fine scan analysis: C1s spectra of (a) GOF and (b) RGF, O1s spectra of (c) ROF and (d) RGF.

Table 2 – Fitted results (%) of C1s XPS spectra of GOF and RGF.

Sample	C–C	C–O	C=O	C(O)O
GOF	39.2	51.2	8.4	1.2
RGF	73.2	18.1	3.6	5.1

Table 3 – Fitted results (%) of O1s XPS spectra of GOF and RGF.

Sample	Quinones	O=C	O–C	O–H
GOF	4.0	22.2	69.2	4.6
RGF	11.6	7.8	3.3	77.3

fied and the C/O atom ratio was remarkably increased from 1.49 of GOF to 17.3 of RGF, which also confirms the removal of oxygen in the film during annealing. A further fitting of C1s and O1s fine scan spectra (Fig. 5) was conducted and the quantified results of different functional species were listed in Tables 2 and 3, respectively. The C1s spectra consists of two main components arising from C–C (∼284.4 eV) and C–O (epoxy and hydroxyl, ∼286.4 eV), and two minor components from C=O (carbonyl, ∼287.8 eV) and O–C=O (carboxyl, ∼288.8 eV), which is similar to other reports [8,39,40]. Comparing with raw GOF, the total contents of oxygen functionalities in the RGF were obviously decreased. The 800 °C annealed RGF shows an obvious decrease in oxygen components (such as C–O, C=O, O–H) with a simultaneous increase in graphitic carbon (such as C–C) (Table 2), and a graphitic shake up peak can thus be observed in the C1s spectra of RGF. The O1s spectra of GO were composed of two major components from C–O (epoxy and hydroxyl, ∼532.5 eV), C=O (carbonyl and carboxyl, ∼531.6 eV), and two minor components for quinones (∼530.5 eV) and O–H (hydroxyl, ∼533.5 eV). After annealing, the normalised intensity of O1s peaks decreased sharply, especially for the contribution from C–O and C=O, indicating the removal of epoxyl, carboxyl, and carbonyl functional groups. The contribution of O–H became the major one, and very few absorbed water at 535.1 eV can be detected on the RGF.

Furthermore, the TG-DSC analysis in both air and argon atmosphere was employed to evaluate the thermal stability and carbonization accessibility of RGF. As shown in Fig. 6, the RGF exhibits a prominent thermal stability in inert argon atmosphere with a very smooth weight loss starting from 800 °C and a residue carbon rate as high as 85% at 1000 °C. Thus, it provides RGF a fertile ground for further self-structural curing by carbonization and re-graphitization at a higher temperature (e.g. over 1200 °C) [41]. However, it remains an open question if the structural integrity of the film is still preserved at these temperatures. Meanwhile, the RGF also exhibits an excellent inflaming retarding performance and the kindling point could reach as high as ∼630 °C in air, which is significantly higher than that of GOF (∼450 °C as shown in Fig. 7).

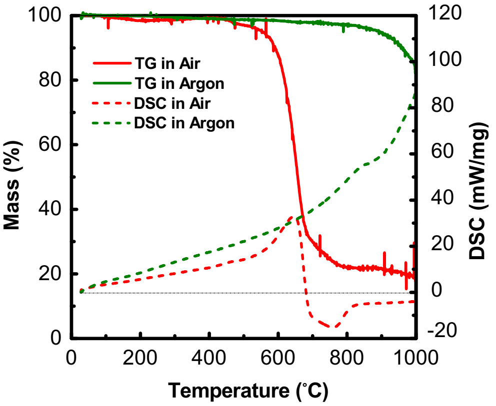

Fig. 6 – TG-DSC analysis of RGF in air and argon atmospheres.

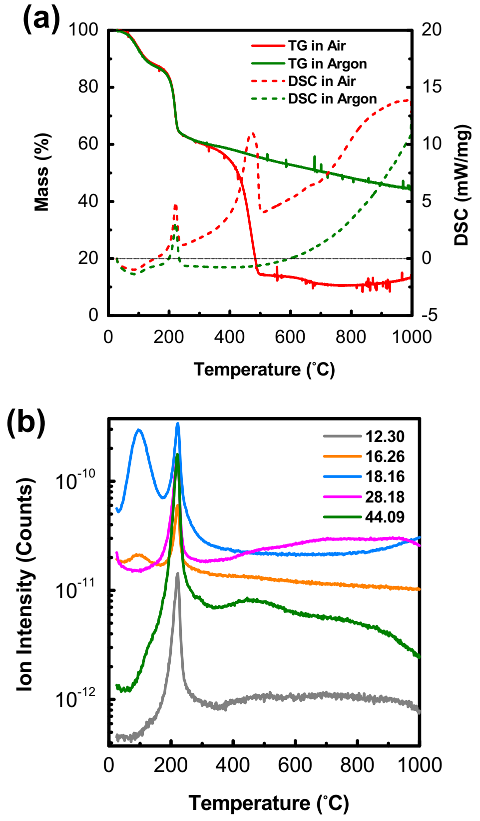

Fig. 7 – (a) TG-DSC analysis of GOF in air and argon and (b) *in situ* MS spectra of sweep gas in the case of argon atmosphere.

In order to monitor the decomposition behavior and chemical transformation of interlayer functional groups in GOF in the whole annealing process, a TG-DSC-mass spectrometry (MS) experiment was performed by annealing GOF to 1000 °C in air and argon with *in situ* sweep gas analysis by MS. As shown in Fig. 7a, the GOF presents a typical 3-stage weight loss pattern in inert atmosphere: (i) 13% weight loss from 0 to 170 °C, with a corresponding peak in MS at 95 °C ($m/z = 18.16$), which can be attributed to the desorption of physically adsorbed interlayer water. The broad endothermic peak around ∼85 °C in DSC pattern indicates the heat adsorbing behavior during water evaporation; (ii) 23% rapid weight loss from 170 to 238 °C, with sharp MS peaks at ∼220 °C for all the listed species in Fig. 7, which can be attributed to the fierce decomposition of oxygen-containing functional groups, and the released small molecules were determined to be H_2O ($m/z = 18.16$), CO ($m/z = 28.18$), CO_2 ($m/z = 44.09$) and radical C ($m/z = 12.30$). The sharp positive peak at 220 °C in DSC confirms the exothermic process due to the bond breaking of functionalities; (iii) 19% smooth weight loss from 238 to 1000 °C, with comparatively steady H_2O and CO_2 but increasing CO molecules releasing, indicating the further deoxygenation from the sp^2 graphitic lattice. Finally, ∼45% of the mass is preserved when the temperature reaches 1000 °C.

Based on above results, the chemical evolution of the film during annealing is schematically illustrated in Fig. 8. As the basic building-blocks of GOF, the individual GO sheet is believed to be jogged of two kinds of crystalline regions: (i) sp^2 regions composed of unoxidized graphitic carbon and (ii) sp^3 regions composed of aliphatic carbon due to the decoration and distorture of graphitic lattice by various oxygen groups (–COOH, –OH, –C=O and epoxy), lattice defects, and dangling bonds. During the thermal annealing of GOF which is closely packed by individual GO sheets, the oxygen containing functional groups (Fig. 8a), such as epoxy, hydroxyl groups were removed as CO, and carboxyl groups were removed as CO_2 [42] with the increasing of temperature under argon atmosphere. During annealing process, carbonyl and ether groups were formed through transformation of the initial hydroxyl and epoxy groups, and the removal of carbon from the graphene plane is more likely to occur when the initial hydroxyl and epoxy groups are in close proximity to each other [43]. From the illustration as shown in Fig. 8a, it is found that the loss of oxygen functional groups and carbon atoms will cause a shrink in the size of sp^2 domains, which is in accordance with the Raman spectra. On the other hand, with the loss of functional groups, the film shrinked and leading to pristine internal stress. If the annealing is taken place in a free space, cracks will generate between graphene sheets and the films will delaminate into twisted debris (Fig. 8b). However, if the film is confined between stacked wafers, the pressure-induced friction between the wafers and GO film would limit the movement of GO flakes, and thus the morphology could be well preserved (Fig. 8c). The improvement of electrical conductivity was highly depended on the structural evolution during the annealing process. In GOF, the introduction of oxygen functionalities to the basal plane and edge of graphene during liquid phase oxidation of graphite causes a disruption of the C–C sp^2 conjugated crystal lattice, and resulting in the loss of conductivity. After annealing, the increased π–π inter-

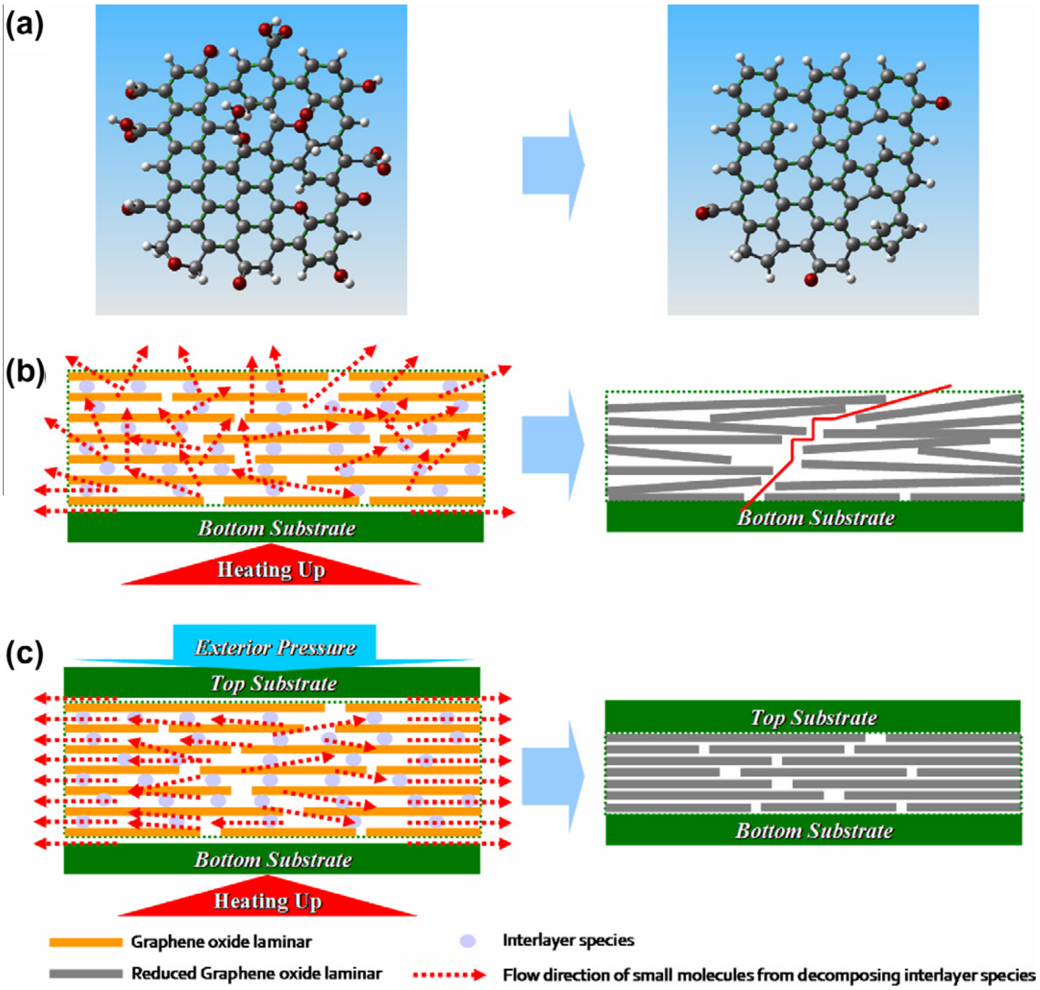

Fig. 8 – Illustration of re-graphitization of GOF into RGF through an annealing process: (a) chemical evolution from GO to graphene; (b) annealing of GOF in an open space; and (c) annealing of GOF in a confined space.

actions between GO and reduced GO sheets, despite a low in-plane conductivity, favors the transport of charge carriers.

4. Conclusions

A highly conductive, free-standing graphene film was obtained by annealing GO film between two stacked wafers. The oxygen-containing functional groups were removed during annealing, which caused the decrease of the sp^2 domains size. The conjugation of the graphene basal plane and π–π interactions between GO and reduced GO sheets favor the transport of charge carriers, and render the free-standing RGF with good electric conductivity. This is an efficient and effective way to fabricate highly conductive RGF in large scale and low cost, which provides graphene macroscopic materials for application exploration.

REFERENCES

[1] Novoselov KS, Geim AK, Morozov SV, Jiang D, Zhang Y, Dubonos SV, et al. Electric field effect in atomically thin carbon films. Science 2004;306(5696):666–9.
[2] Guo SJ, Dong SJ. Graphene nanosheet: synthesis, molecular engineering, thin film, hybrids, and energy and analytical applications. Chem Soc Rev 2011;40(5):2644–72.
[3] Xu YX, Shi GQ. Assembly of chemically modified graphene: methods and applications. J Mater Chem 2011;21(10):3311–23.
[4] Zhu YW, Murali S, Cai WW, Li XS, Suk JW, Potts JR, et al. Graphene and graphene oxide: synthesis, properties, and applications. Adv Mater 2010;22(35):3906–24.
[5] Dikin DA, Stankovich S, Zimney EJ, Piner RD, Dommett GHB, Evmenenko G, et al. Preparation and characterization of graphene oxide paper. Nature 2007;448(7152):457–60.
[6] Chen CM, Yang QH, Yang YG, Lv W, Wen YF, Hou PX, et al. Self-assembled free-standing graphite oxide membrane. Adv Mater 2009;21(29):3007–11.
[7] Kim F, Cote LJ, Huang JX. Graphene oxide: surface activity and two-dimensional assembly. Adv Mater 2010;22(17):1954–8.
[8] Xu YX, Bai H, Lu GW, Li C, Shi GQ. Flexible graphene films via the filtration of water-soluble noncovalent functionalized graphene sheets. J Am Chem Soc 2008;130(18):5856–7.
[9] Park S, Mohanty N, Suk JW, Nagaraja A, An JH, Piner RD, et al. Biocompatible, robust free-standing paper composed of a TWEEN/graphene composite. Adv Mater 2010;22(15):1736–40.
[10] Liu F, Seo TS. A controllable self-assembly method for large-scale synthesis of graphene sponges and free-standing graphene films. Adv Funct Mater 2010;20(12):1930–6.
[11] Yang XW, Zhu JW, Qiu L, Li D. Bioinspired effective prevention of restacking in multilayered graphene films: towards the next generation of high-performance supercapacitors. Adv Mater 2011;23(25):2833–8.
[12] Xu YX, Sheng KX, Li C, Shi GQ. Self-assembled graphene hydrogel via a one-step hydrothermal process. ACS Nano 2010;4(7):4324–30.
[13] Lee SH, Kim HW, Hwang JO, Lee WJ, Kwon J, Bielawski CW, et al. Three-dimensional self-assembly of graphene oxide platelets into mechanically flexible macroporous carbon films. Angew Chem Int Ed 2010;49(52):10084–8.
[14] Tang ZH, Shen SL, Zhuang J, Wang X. Noble-metal-promoted three-dimensional macroassembly of single-layered graphene oxide. Angew Chem Int Ed 2010;49(27):4603–7.
[15] Chen ZP, Ren WC, Gao LB, Liu BL, Pei SF, Cheng HM. Three-dimensional flexible and conductive interconnected graphene networks grown by chemical vapour deposition. Nat Mater 2011;10(6):424–8.
[16] Liu QF, Ishibashi A, Fujigaya T, Mimura K, Gotou T, Uera K, et al. Formation of self-organized graphene honeycomb films on substrates. Carbon 2011;49(11):3424–9.
[17] Fan ZJ, Yan J, Zhi LJ, Zhang Q, Wei T, Feng J, et al. A three-dimensional carbon nanotube/graphene sandwich and its application as electrode in supercapacitors. Adv Mater 2010;22(33):3723–8.
[18] Lv RT, Cui TX, Jun MS, Zhang Q, Cao AY, Su DS, et al. Open-ended, N-doped carbon nanotube-graphene hybrid nanostructures as high-performance catalyst support. Adv Funct Mater 2011;21(5):999–1006.
[19] Chen CM, Yang YG, Wen YF, Yang QH, Wang MZ. Preparation of ordered graphene-based conductive membrane. New Carbon Mater 2008;23(4):345–50.
[20] Pham VH, Cuong TV, Hur SH, Shin EW, Kim JS, Chung JS, et al. Fast and simple fabrication of a large transparent chemically-converted graphene film by spray-coating. Carbon 2010;48(7):1945–51.
[21] Xu YF, Long GK, Huang L, Huang Y, Wan XJ, Ma YF, et al. Polymer photovoltaic devices with transparent graphene electrodes produced by spin-casting. Carbon 2010;48(11):3308–11.
[22] Li XL, Zhang GY, Bai XD, Sun XM, Wang XR, Wang E, et al. Highly conducting graphene sheets and Langmuir–Blodgett films. Nat Nanotechnol 2008;3(9):538–42.
[23] Schniepp HC, Li JL, McAllister MJ, Sai H, Herrera-Alonso M, Adamson DH, et al. Functionalized single graphene sheets derived from splitting graphite oxide. J Phys Chem B 2006;110(17):8535–9.
[24] Eda G, Fanchini G, Chhowalla M. Large-area ultrathin films of reduced graphene oxide as a transparent and flexible electronic material. Nat Nanotechnol 2008;3(5):270–4.
[25] Yang D, Velamakanni A, Bozoklu G, Park S, Stoller M, Piner RD, et al. Chemical analysis of graphene oxide films after heat and chemical treatments by X-ray photoelectron and Micro-Raman spectroscopy. Carbon 2009;47(1):145–52.
[26] Stankovich S, Dikin DA, Piner RD, Kohlhaas KA, Kleinhammes A, Jia Y, et al. Synthesis of graphene-based nanosheets via chemical reduction of exfoliated graphite oxide. Carbon 2007;45(7):1558–65.
[27] Xu YX, Sheng KX, Li C, Shi GQ. Highly conductive chemically converted graphene prepared from mildly oxidized graphene oxide. J Mater Chem 2011;21(20):7376–80.
[28] Shin HJ, Kim KK, Benayad A, Yoon SM, Park HK, Jung IS, et al. Efficient reduction of graphite oxide by sodium borohydrilde and its effect on electrical conductance. Adv Funct Mater 2009;19(12):1987–92.
[29] Pei SF, Zhao JP, Du JH, Ren WC, Cheng HM. Direct reduction of graphene oxide films into highly conductive and flexible graphene films by hydrohalic acids. Carbon 2010;48(15):4466–74.
[30] Fan ZJ, Wang K, Wei T, Yan J, Song LP, Shao B. An environmentally friendly and efficient route for the reduction of graphene oxide by aluminum powder. Carbon 2010;48(5):1686–9.
[31] Gao W, Alemany LB, Ci LJ, Ajayan PM. New insights into the structure and reduction of graphite oxide. Nat Chem 2009;1(5):403–8.
[32] Hummers WS, Offeman RE. Preparation of graphitic oxide. J Am Chem Soc 1958;80(6):1339.
[33] Liu YZ, Li YF, Yang YG, Wen YF, Wang MZ. The effect of thermal treatment at low temperatures on graphene oxide films. New Carbon Mater 2011;26(1):41–5.

[34] Moon IK, Lee J, Ruoff RS, Lee H. Reduced graphene oxide by chemical graphitization. Nat Commun 2010;1:73.

[35] Liu J, Jeong H, Liu J, Lee K, Park JY, Ahn YH, et al. Reduction of functionalized graphite oxides by trioctylphosphine in non-polar organic solvents. Carbon 2010;48(8):2282–9.

[36] Liu JQ, Lin ZQ, Liu TJ, Yin ZY, Zhou XZ, Chen SF, et al. Multilayer stacked low-temperature-reduced graphene oxide films: preparation, characterization, and application in polymer memory devices. Small 2010;6(14):1536–42.

[37] Lai LF, Chen LW, Zhan D, Sun L, Liu Jp, Lim SH, et al. One-step synthesis of NH_2-graphene from *in situ* graphene-oxide reduction and its improved electrochemical properties. Carbon 2011;49(10):3250–7.

[38] An SJ, Zhu YW, Lee SH, Stoller MD, Emilsson T, Park S, et al. Thin film fabrication and simultaneous anodic reduction of deposited graphene oxide platelets by electrophoretic deposition. J Phys Chem Lett 2010;1(8):1259–63.

[39] Peng X-Y, Liu X-X, Diamond D, Lau KT. Synthesis of electrochemically-reduced graphene oxide film with controllable size and thickness and its use in supercapacitor. Carbon 2011;49(11):3488–96.

[40] Yan J, Wei T, Shao B, Ma FQ, Fan ZJ, Zhang ML, et al. Electrochemical properties of graphene nanosheet/carbon black composites as electrodes for supercapacitors. Carbon 2010;48(6):1731–7.

[41] Oberlin A. Carbonization and graphitization. Carbon 1984;22(6):521–41.

[42] Figueiredo JL, Pereira MFR, Freitas MMA, Orfao JJM. Modification of the surface chemistry of activated carbons. Carbon 1999;37(9):1379–89.

[43] Bagri A, Mattevi C, Acik M, Chabal YJ, Chhowalla M, Shenoy VB. Structural evolution during the reduction of chemically derived graphene oxide. Nat Chem 2010;2(7):581–7.